3

Detection of High Quality Parts of Hydrocarbon Reservoirs Using Bayesian Facies Estimation: A Case Study on a Carbonate Reservoir from Iran

3

Detection of High Quality Parts of Hydrocarbon Reservoirs Using Bayesian Facies Estimation: A Case Study on a Carbonate Reservoir from Iran

Sadegh Karimpouli[1], Hossein Hassani[2], Hossein Khoshdel[3], Alireza Malehmir[4], Majid Nabi-Bidhendi[5]

[1]Department of Mining Engineering, University of Zanjan, Zanjan, Iran. Email: s_karimpouli@znu.ac.ir

[2]Faculty of Mining and Metallurgy Engineering, Amirkabir University of Technology, Tehran, Iran. Email: hhassani@aut.ac.ir

[3]Exploration Directorate, NIOC, Tehran, Iran. Email: hkhoshdel@yahoo.com

[4]Department of Earth Sciences, Uppsala University, SE 75236 Uppsala, Sweden Email: alireza.malehmir@geo.uu.se

[5]Institute of Geophysics, University of Tehran, Tehran, Iran. Email: mnbhendi@ut.ac.ir

Summary

Quality of a reservoir can be described by its petrophysical properties which depend on the reservoir type and differ from sandstone to carbonate type reservoirs. For a given mineral composition and a fluid type, the complexity of carbonate pore types affects reservoir permeability heterogeneity and seismic velocity variation more strongly than porosity does. Therefore, porosity, frame flexibility factor (which describes the pore types) and bulk modulus of fluid are suggested as the proper petrophysical parameters that define facies with different qualities in a carbonate reservoir. A high quality facies is, then, a high porous facies with proper pore type containing gas as fluid content. Conversely, a low quality facies is the low porous one with improper pore type containing brine. Finally, the transition facies is the one between these two end members. A complete version of

Bayesian facies inversion can be used to locate the high quality parts of the reservoir. In this study, petrophysical parameters were obtained using well logs and core data from a well located in the study area. The mentioned facies were defined on the basis of the Gaussian mixture distribution of data in a 3D space of petrophysical parameters. Subsequently, 3D prestack migrated seismic data in different angles were used to predict high quality facies along the reservoir. The results show that K2 and K4 are two high quality reservoir levels which were previously introduced by geochemical and sedimentological studies.

3.1 Introduction

The term ''facies'' is used for categorical groups - not necessarily only for a lithology type but also for some properties or collections of properties, as, for example, a combination of lithology and pore fluids (Bosch et al., 2010). A facies can also be defined as though it introduces the quality of a reservoir. Bayesian inversion was developed during the last decade to invert the desired facies from seismic data in a statistical approach. The aim of the inversion from a statistical point of view is not only to find a best-fitting set of model parameters but also to characterize the uncertainty in the inversion results (Buland, 2002). A Bayesian setting is a natural choice for probabilistic classification and geophysical inverse problems, where it is possible to combine available prior knowledge with the information contained in the measured data (Ulrych et al., 2001; Buland and More, 2003; Tarantola, 2005). The solution of a Bayesian inverse problem is represented by the posterior distribution. Since the probability of solution can be easily calculated, uncertainties are also captured.

Mukerji et al. (2001) introduced statistical rock physics to estimate sandstone reservoir parameters and used the Bayesian classification to evaluate uncertainty from pre-stack seismic data. Buland and Omre (2003) presented an analytical

Bayesian-linearized AVO inversion to invert elastic rock parameters (P- and S-wave velocities and density). The importance of this method is that an explicit analytical form is usually computationally superior to an iterative search and simulation-based solutions (Buland and Omre, 2003). Houck (2002) estimated uncertainty using an approach based on Bayes's rule, combining pertinent geologic and geophysical AVO information. Eidsvik et al. (2004), Larsen et al. (2006) and Ulvmoen and Omre (2010) predicted lithology-fluid of a sandstone reservoir using Markov random fields in a Bayesian framework. Buland et al. (2008) developed their Bayesian method to predict the most probable facies. Grana and Della Rossa (2010) and Karimpouli et al. (2013) have recently presented a more complete version of the Bayesian inversion of facies from prestack seismic data. They combined three conditional distributions with a Bayesian classification to estimate the rock physics parameters and probability of different facies with the evaluation of the associated uncertainties.

The definition of ''a facies'' is based on petrophysical parameters. A combination of these parameters can introduce the quality of the reservoir. However, the point is that petrophysical parameters depend on reservoir types. In sandstone reservoirs, porosity, water saturation and clay content are known as common parameters describing the quality of a reservoir. Desired facies can be defined and estimated according to these parameters (see Grana and Della Rossa, 2010). However, the estimation of rock properties is much more challenging in carbonate rocks because of their strong heterogeneity. This implies that other parameters, which cause heterogeneity, must be considered too. The first step, in these kinds of studies, is usually the determination of proper parameters describing the complicated behaviors of carbonate rocks. These complexities depend on their mineralogy, fluid content, porosity, pore type and structure, pressure, and temperature (Sun, 2004). They also cause seismic responses to be more ambiguous in rock physics parameters prediction than in sandstone rocks.

The main reason for such ambiguities in the elastic behaviors of carbonate rocks can be understood in their tendency to have highly variable and complicated pore systems which often results from their formation processes (Anselmetti and Eberli, 1999; Assefa et al., 2003; Eberli et al., 2003; Adam et al., 2006; Baechle et al., 2009; Saberi, 2010). Porosity and pore types are the main parameters that control velocity, whereby variation in pore type is the main reason for variable velocity at a given porosity (Eberli et al., 2003). For a given mineral composition and a fluid type, the complexity of its carbonate pore types, such as moldic, vuggy, interparticle, intraparticle, crack and others, affects reservoir permeability heterogeneity and seismic velocity variation more strongly than porosity does (Anselmetti and Eberli, 1999; Dou et al., 2009a, b; Dou et al., 2011). For example, pore type variations can make seismic compressional velocity differ by 2.5 km/s or even greater for a given constant porosity (Sun, 2004). Thus, there must be a rock physics model to evaluate the pore type variation, and to relate the pore space type and structure to other rock parameters. Sun (2000, 2004) and Sun and Goldberg (1997a, b) introduced a rock physics model based on a dynamic theory of fractured porous media by extending the Biot theory. Sun (2000) defined the elastic parameter as a frame flexibility factor that depends less on the porosity than wave velocities do. Meanwhile, this parameter is not only related to pore structure variation but also to solid/pore connectivity and rock texture in carbonate reservoirs (Sun, 2004). This poroelasticity model was proven at the core and log scales in its effectiveness in quantifying pore structure, and it was successfully used for carbonate reservoir parameter inversion from seismic data (Dou et al., 2011). Thus, porosity and frame flexibility factor were chosen as proper parameters in carbonate reservoir studies. In this study, to delineate the fluid type, we chose the bulk modulus of fluid as the third parameter for three reasons. First, we are exploring the gas in this reservoir and the large contrast of this parameter (i.e., bulk modulus of fluid) between gas and water (or oil) making

it possible to be used for fluid type delineation. Second, the classification method used in this study is based on the separation of different distributions; we observed well-separated distributions using bulk modulus of fluid. Third, the rock physics model for the frame flexibility factor contains this parameter; which means it can easily be predicted. Consequently, we proposed porosity, frame flexibility factor, and bulk modulus of fluid as the proper parameters to define and estimate facies in carbonate reservoirs.

In this paper, a gas field from Iran is studied. The field is well known for its important gas-bearing carbonate reservoirs; nevertheless, more accurate interpretation of seismic data is in high demand for future exploration phases. Our objectives in this study are to determine gaseous facies from seismic data, to find their distribution at the reservoir zone, and to calculate probability of their occurrences. Knowledge about these properties can play a crucial role for future planning of exploration and production phases. After a brief introduction about the geological setting in the study area, we show how we obtained the mentioned rock physics parameters from available data.

3.2 Methodology of Bayesian Facies Inversion

Suppose that S is the observed seismic data, m is the matrix of elastic parameters of the rock such as velocities or seismic impedances, R is the matrix containing petrophysic parameters such as porosity, water saturation, etc., and, finally, f is the desired facies. The probability of facies occurrence in depth z conditioned to the observed seismic data ($P(f_z \mid S_z)$) can be related to petrophysical parameters with Chapman-Kolmogorov relation:

$$P(f_z \mid S_z) = \int_R P(f_z \mid R) P(R \mid S_z) dR \tag{1}$$

where $P(f_z|R)$ and $P(R|S_z)$ are distribution of facies conditioned to petrophysical parameters and probability of petrophysical parameters conditioned to the observed seismic data in depth *z*, respectively. The Chapman-Kolmogorov relation can also be used to relate eq. (1) to elastic parameters of the rock:

$$P(fR|S_z) = \int_m P(R|m)P(m|S_z)dm \tag{2}$$

$$P(f_z|S_z) = \int_R \int_m P(f_z|R)P(R|m)P(m|S_z)dmdR \tag{3}$$

where $P(m|S_z)$ distribution of elastic parameters, conditioned to the observed seismic data and can be obtained using Bayesian linearized AVO inversion by Buland and Omre (2003). On the other hand, $P(R|m)$ is the distribution of petrophysical parameters conditioned to elastic parameters and can be calculated using probabilistic inversion of petrophysical models (Grana and Della-Rossa, 2010). The most important point is that the elastic parameters, inverted from seismic data, and petrophysical parameters, obtained from well log data, have different scales. The well log scale which is in the order of 10 centimeters must be accounted by up-scaling methods to the seismic scale which is in the order of 10 meters. $P(f_z|R)$ is the distribution of facies conditioned to the petrophysical parameters determined by classification of petrophysical data distributions. The relation of all these probability functions is illustrated in Figure 1. All of these steps are described in the following sections.

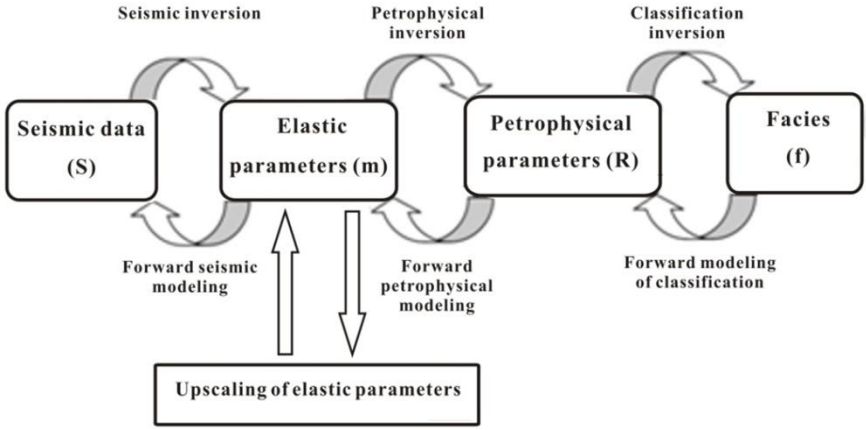


Figure 1. *Schematic diagram of facies inversion from seismic data. S are the seismic data at depth z. The earth model response is assumed to be isotropic with three elastic parameters consisting of P- and S-wave velocity and density which are denoted by m. In practice, other derivations of elastic parameters such as seismic impedances can also be used. R is representative of petrophysical parameters (Modified from Karimpouli et al., 2013).*

3.2.1 Bayesian Linearized AVO Inversion

Buland and Omre (2003) introduced an analytical version of Bayesian linearized AVO inversion to obtain posterior distribution of elastic parameters. The inversion method assumes an isotropic medium with P- and S-wave velocities and density as elastic parameters, and used a convolutional model of Aki and Richards (1980) linearized approximation of the Zoeppritz equation that is valid for vertical, and weak contrasts. Since the inversion cannot retrieve reliable information about the density, another approximation based on P- and S-wave impedances can be used as a forward model:

$$R_{PP}(\theta) \approx \frac{1}{2Cos^2\theta}\frac{\Delta I_P}{\bar{I}_P} - 4\frac{\bar{I}^2_S}{\bar{I}^2_P}Sin^2\theta\frac{\Delta I_S}{\bar{I}_S} + \left(\frac{1}{2} - \frac{1}{2Cos^2\theta} + 2\frac{\bar{I}^2_S}{\bar{I}^2_P}Sin^2\theta\right)\frac{\Delta\rho}{\bar{\rho}} \quad (4)$$

where I_P, I_S are P- and S-wave impedances and θ is the incident angle of the seismic wave. The forward model for seismic data using logarithmic elastic parameters (m_l) is:

$$S = Gm_l + e \tag{5}$$

where $m = [I_P, I_S]^T$ and G is the operator of linearized forward modelling (data kernel). $G = WAD$ (refer to Buland et al., 2008) and e is a Gaussian error term with zero mean and covariance $\sum e$. $P(m_l)$ is the prior distribution in the Bayesian framework which is assumed to be multivariate Gaussian with mean μ_{m_l} and covariance matrix $\sum m_l$:

$$P(m_l) \sim N(m_l, \mu_{m_l}, \sum m_l) \tag{6}$$

Therefore, the data obtained from forward modelling have also Gaussian distribution with mean μ_S and covariance matrix $\sum S$:

$$P(S) \sim N(S, \mu_S, \sum S) \tag{7}$$

The joint probability distribution function of elastic parameters and forward modelling can be written as:

$$P\left(\begin{bmatrix} m_l \\ S \end{bmatrix}\right) \sim N\left(\begin{bmatrix} m_l \\ S \end{bmatrix}; \begin{bmatrix} \mu_{m_l} \\ \mu_S \end{bmatrix}, \begin{bmatrix} \sum m_l & \sum m_l, S \\ \sum S, m_l & \sum S \end{bmatrix}\right) \tag{8}$$

where $\sum S, m_l = \sum m_l, S$ are cross correlation of m and S. Because a Gaussian distribution is a closed distribution, the posterior distribution is again Gaussian:

$$P(m_l \mid S) \sim N(m_l; \mu_{m_l|S}, \sum m_l \mid S) \tag{9}$$

$$\mu_{m_l|S} = \mu_{m_l} + \left(G \sum m_l\right)^T \sum S^{-1} (S - \mu_S) \tag{10}$$

$$\sum m_l \mid S = \sum m_l + \left(G\sum m_l\right)^T \sum S^{-1} G \sum m_l \tag{11}$$

And finally, $P(m_l \mid S_z)$ can be calculated using lognormal transformation of $P(m_l \mid S)$ at each vertical position *z*.

3.2.2 Statistical Petrophysical Modelling

One of the most important aspects of statistical petrophysics is that it combines petrophysical models with statistical studies and, therefore, it is possible to obtain some information about the situations which are not seen in well log data (Avseth et al., 2001). With the assumption that petrophysical parameters are random variables, a petrophysical model can be written as:

$$m = g(R) + e \tag{12}$$

where e is the error representing the accuracy of the model with zero mean and covariance $\sum e$. The covariance matrix of error model can be calculated from the well log data.

The next step is estimation of probability distribution of petrophysical parameters. The main problem is that these parameters do not have Gaussian distribution. The normality assumption is a strong limitation present in many existing approaches. To overcome this problem, Gaussian mixture distribution is proposed to be used to describe the non-Gaussian behavior of the desired rock properties (Grana and Dvorkin, 2011). This choice is motivated by two reasons. First, this formulation allows us to model each facies class detectable from a petrophysical point of view as a single Gaussian component of the mixture. Second, the approach is analytically convenient because the analytical results valid for Gaussian distributions can also be extended to Gaussian mixtures (Grana and Dell Rossa, 2010).

$$P(R)=\sum_{k=1}^{N_c}\alpha_k N\left(R;\mu_R^k,\sum{}_R^k\right) \tag{13}$$

where $\mu_R^k,\sum{}_R^k$ are mean and covariance matrix of Gaussian mixture distribution of $\sum{}_R^k$ for $k=1...N_c$, where N_c is the number of distribution components and α_k are corresponding weights of linear combination of components ($\sum_{k=1}^{N_c}\alpha_k=1$). Therefore:

$$P(m\mid R)=N(m;\mu(R),\sum e) \tag{14}$$

where $\mu(R)=g(R)$ and the covariance matrix is independent from R and is related just to the distribution of error terms. This model allows us to evaluate uncertainty of the model using Monte Carlo methods and conditional probability distributions. $P(m\mid R)$ can be calculated in a semi-analytical approach as follows (Grana and Della Rossa, 2010):

(1) Generating a set of k samples $\{R_i, i=1,...,k\}$ according to $P(R)$ which is a Gaussian mixture by Monte Carlo simulation.

(2) Applying petrophysical models to each sample and calculating $N(m;\mu(R),\sum e)$ for them.

(3) Generating l samples $\{m_j, j=1,...,l\}$ from all of the distributions calculated in the previous step and making the joint Gaussian mixture distribution $P(m,R)$.

$$P(m,R)=\sum_{k=1}^{N_c}\pi_k N\left([m,R]^T;\mu_{[m,R]}^k,\sum\nolimits_{[m,R]}^k\right) \tag{15}$$

(4) Computing conditional distribution $P(m\mid R)$:

$$P(m\mid R)=\sum_{k=1}^{N_c}\gamma_k N\left(m;\mu_{R|m}^k,\sum\nolimits_{R|m}^k\right) \tag{16}$$

$$\mu_{R|m}^k=\mu_R^k+\sum\nolimits_{R,m}^k\left(\sum\nolimits_{m,m}^k\right)^{-1}(m-\mu_m^k) \tag{17}$$

$$\sum\nolimits_{R|m}^k=\sum\nolimits_{R,R}^k-\sum\nolimits_{R,m}^k\left(\sum\nolimits_{m,m}^k\right)^{-1}\sum\nolimits_{m,R}^k \tag{18}$$

$$\gamma_k(m)=\frac{\alpha_k N(R;\mu_{R|m}^k,\sum\nolimits_{R|m}^k)}{\sum_{l=1}^{N_c}\gamma_l N(R;\mu_{R|m}^l,\sum\nolimits_{R|m}^l)} \tag{19}$$

3.2.3 Probabilistic Up-Scaling

Different sources of information cause a difference in scale between seismic and well data (coarse and fine scale). Up-scaling means to replace a heterogeneous volume with a homogeneous volume having effectively equivalent elastic constants (Tiwary et al., 2007). Seismic data contain the properties at the scale of tens of meters whereas well data contain properties at the scale of a few to several centimeters. This means an average effect of several sets of data at well scale can be equivalent to one set of data at the seismic scale. Backus (1962) obtained the exact solution to calculate the effective properties for a layered medium using the assumption that all constituents of the medium are linearly elastic and isotropic and that there is no source of energy dissipation because of friction or viscosity. Therefore, elastic parameters in well scale (m^w) can be related to the seismic scale (m^s) as:

$$m^s = g(m^w) \tag{20}$$

Grana and Della Rossa (2010) proposed a method using Backus (1962) averaging which defines a probabilistic step to account for the up-scaling part in the following steps:

(1) Generating a set of l samples $\left\{m_i^w, i=1,...,l\right\}$ according to $P(m^w \mid R)$ by Monte Carlo simulation.

(2) Applying Backus up-scaling and obtaining elastic properties at the seismic scale m^s.

(3) Estimating conditional distribution $P(m^w \mid m^s)$ from the joint distribution of $\left\{m_i^w, m_i^s\right\}$.

(4) Applying Chapman-Kolmogorov equation:

$$P(R \mid m^s) = \int_{m^w} P(R \mid m^w) P(m^w \mid m^s) dm^w \tag{21}$$

3.2.4 Facies Classification a Prior Model

Facies distribution conditioned to the petrophysical parameters is:

$$P(f_z \mid R) = \frac{P(R \mid f_z) P(f_z)}{P(R)} = C \times P(R \mid f_z) P(f_z) \tag{22}$$

where C is the constant.

The denominator in eq. (22) is constant and is not related to the facies occurrence (Duijndam 1988, Ulrych et al., 2001). $P(R \mid f_z)$ is the distribution of petrophysical parameters conditioned to a determined facies and can be

accounted as classification inversion in Figure 1. The number of components in Gaussian mixture distribution can be related to the number of facies because it is supposed that each facies in the reservoir has the same petrophysical properties and since these properties differ from one facies to another, corresponding seismic responses are also different. Available information about the number of facies according to the well and core data can be helpful in choosing the number of distribution components.

$P(f_z)$ is the prior probability distribution of facies. It can be presented using Markov chain prior model as:

$$P(f_z) = \prod_z P(f_z \mid f_{z-1}) \tag{23}$$

Where $P(f_1) = P(f_1 \mid f_0)$. The probability of $P(f_z \mid f_{z-1})$ can be obtained by the Markov chain transition matrix using well data.

3.2.5 General Relation

According to the previous sections and by substitution of eqs. (20 and 23) in eq. (3), a complete version of this method is presented:

$$P(f_z \mid S_z) \propto \prod_z P(f_z \mid f_{z-1}) \int_R \int_{m^w} \int_{m^s} P(R \mid f_z) P(R \mid m^w) P(m^w \mid m^s) P(m^s \mid S_z) dm^s dm^w dR \tag{24}$$

Graphical illustration of this equation is shown in Figure 2. The main steps of this method are: (1) Seismic inversion, (2) Petrophysical inversion, and (3) Facies inversion using classification of the well data.

3.3 General Geology and Data

Our study area is a reservoir from South Pars field, the largest gas field in the world, located in the Persian Gulf. Structurally, the field is a part of the Qatar-South Pars arch which is a regional anticline with gentle limbs considered as a basement-cored structure with long lasting passive folding induced by salt withdrawal.

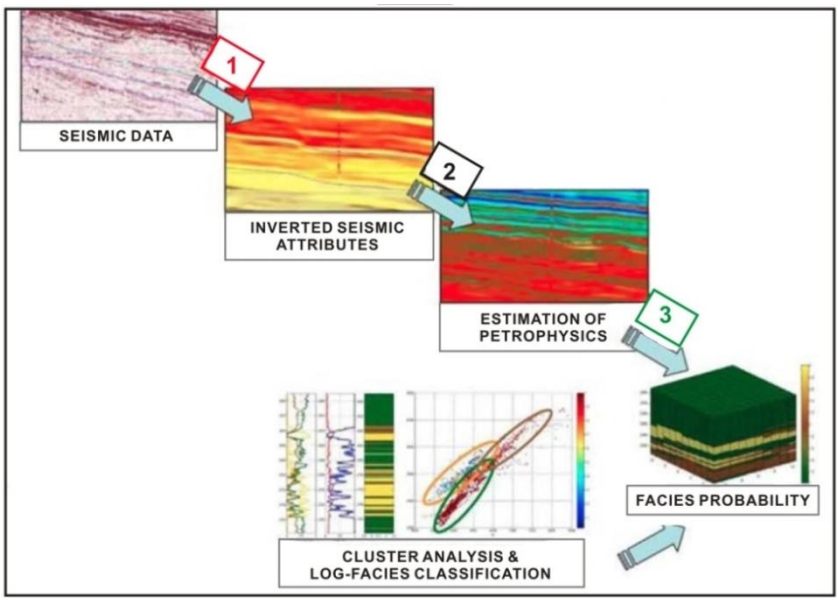


Figure 2. *Flowchart of Bayesian facies inversion.*
(Modified from Roncarolo and Grana, 2010).

Several reservoirs (oil and gas) have been identified in the South Pars field by seismic exploration and appraisal wells. The oil reservoirs are located in the Khami and Bangestan Groups formations (personal communication, National Iran Oil Company (NIOC) 2012). The gas-bearing reservoir belongs to the Kangan and Dalan formations of Triassic and Permian age, respectively. The Aghar Shale of Dashtak formation directly overlies the Kangan formation, which

is the actual seal of the gas accumulation (personal communication NIOC 2012).

Kangan and Dalan formations, known as Khuff formation in the Arabian plate (Tavakoli et al., 2011), host the main production zones. Kangan is divided into two submembers: K1 and K2. Dominant lithology of K1 is anhydritic dolomite, dolomite and limestones while limestones and dolomites are the main lithology of K2. Dalan is divided into four submembers (K3, K4, Nar and K5) two of which are productive: K3 and K4. The K3 is mainly dolomite with lesser amounts of dolomitic limestone and dominant lithology of K4 being dolomite and limestone with some anhydrite intervals. However, Nar is known as the median anhydrite (Figure 3).

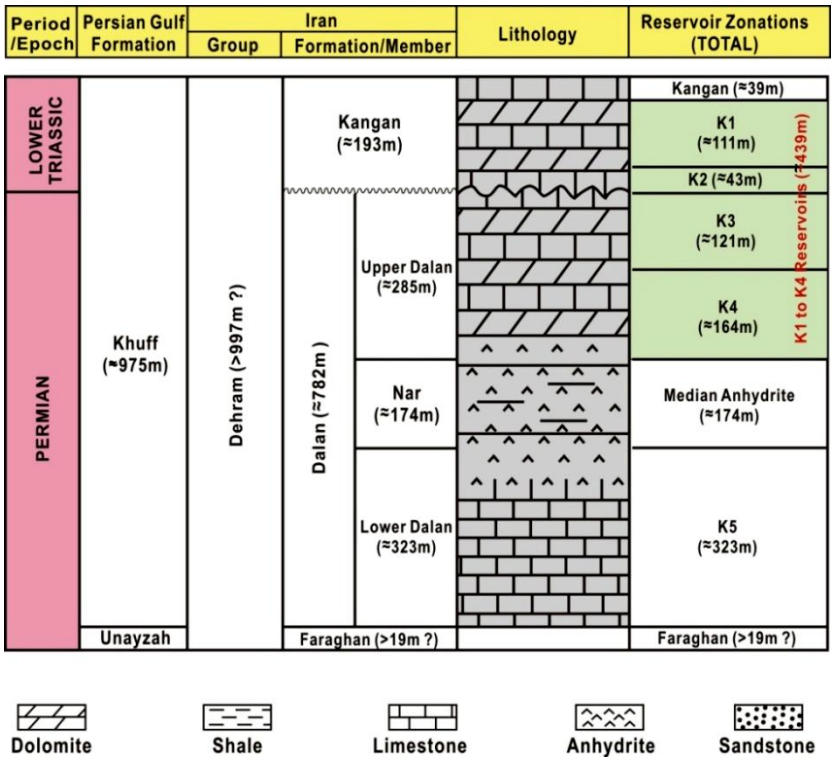


Figure 3. *Sub-members of Kangan and Dalan formations. K1 to K4 are reservoir zones (modified from NIOC, 2003-2004).*

Available data from this study are 3D prestack migrated seismic data and two wells (A, and B). In this study, we directly used well-A in our inversion scheme, but well-B was used for the validation of the inversion results. Well data include special core analysis (SCAL) and core images which were used for determination of lithology and pore space types, and petrophysical measurements such as resistivity, porosity, density, water saturation, mineral percentages, and P- and S-wave velocities.

3.4 Carbonate Reservoir Parameters

Eberli et al. (2003) suggest that porosity and pore types are the main parameters that control seismic velocities in carbonate rocks, whereby variation in pore type is the main reason for variable velocity at a given constant porosity. Depositional environments define depositional textures of the sediments, while subsequent diagenetic alterations modify these textures and create complex rock properties such as porosity and pore type (Anselmetti and Eberli 1999; Saberi, 2010). Sun (2000, 2004) developed a topological characterization of structural media and investigated the general mechanics and thermodynamics of fractured porous media. One of the major developments in Sun's mathematical theory of fractured porous media is direct quantification of the profound effect of pore structure and its connectivity on the elastic properties of rocks. He used the frame flexibility factor (γ) to characterize the effect of pore structure, grain contacts, grain coupling, cementation and pore connectivity on the flexibility and elasticity of porous rocks. It is found that moldic or vuggy pore spaces tend to be rounded and make rock hard; however, interparticle pore spaces or cracks tend to be flat and make rock soft (Dou et al., 2011). Consequently, a seismicwave propagates faster in rocks dominated by moldic and vuggy pore

spaces than it does in rocks with inter-particle pore spaces or cracks (Sun 2004; Dou et al., 2011). According to Sun (2000, 2004) and Dou et al. (2011), the formulation of the bulk frame flexibility factor is as follows. Let V_P, V_S and ρ be compressional velocity, shear velocity and bulk density, respectively. Let K and μ be the bulk and shear moduli of standard rock, respectively:

$$\gamma = 1 + \frac{\ln(f)}{\ln(1-\phi)} \tag{25}$$

where:

$$f = \frac{1 - \left(\frac{K_f}{K_s} + \left(1 - \frac{K_f}{K_s} \right) \phi \right) F_K}{(1-\phi)\left(1 - \frac{K_f}{K_s} F_K \right)} \tag{26}$$

$$F_K = \frac{K_s - K}{\phi (K_s - K_f)} \tag{27}$$

$$K = \left(V_P^2 - \frac{4}{3} V_S^2 \right) \rho \tag{28}$$

$$K = \frac{K_s \left[(1-\phi)^\gamma (\phi K_f - \phi K_s + K_f) - K_f \right]}{K_f (1-\phi)^\gamma - K_f + (K_f - K_s)^\phi} \tag{29}$$

$$\mu = \mu_s (1-\phi)^{d\gamma} \tag{30}$$

where γ is the frame stiffness factor, ϕ porosity, K_f fluid bulk modulus, K_s solid matrix bulk modulus, μ_s solid matrix shear modulus and d gamma ratio of the shear frame flexibility factor γ_μ to the bulk frame flexibility factor γ_K.

The mineral composition of the reservoir zone is dominantly calcite and

dolomite with some anhydrite. Table 1 summarizes the main mineralogical components of the reservoir and their corresponding water saturation value estimated from available well data. The bulk modulus of the matrix (K_s) is calculated using the Voigt-Reuss-Hill mixing model if the percentage of mineral compositions is available (Mavko et al., 2009).

Table 1. *Main mineralogical components of the reservoir and their corresponding water saturation value estimated from available well data.*

Layers	Thickness (m)	Anhydrite (%)	Calcite (%)	Dolomite (%)	Illite (%)	Sw (%)
K1	105	20.18	28.68	49.88	1.26	48.62
K2	47	1.47	40.58	57.41	0.54	18.47
K3	120	19.85	24.64	51.20	4.32	75.02
K4	153	0.64	60.67	35.25	3.44	15.58

In this study, we used the well-log data and calculated the K_s for all points measured in the well. Because this reservoir is a gas-bearing type, there are just two fluid phases: gas and brine. Therefore, we considered a variable bulk modulus of fluid (K_f) and calculated it using the Reuss-Brie average model, since a more effective range will fall roughly between Reuss and Brie averages (Mavko et al., 2009). Four dominant pore space types (PST) were observed in the laboratory by studying the well core samples: vuggy and micro-porosity as the primary porosities which were made when the carbonate rocks were forming (Figures 4(A) and (C)). Cracks and fractures were considered the secondary porosities and were made by diagenetic processes and dominant tectonic regime of the reservoir (Figures 4(B) and (D)).

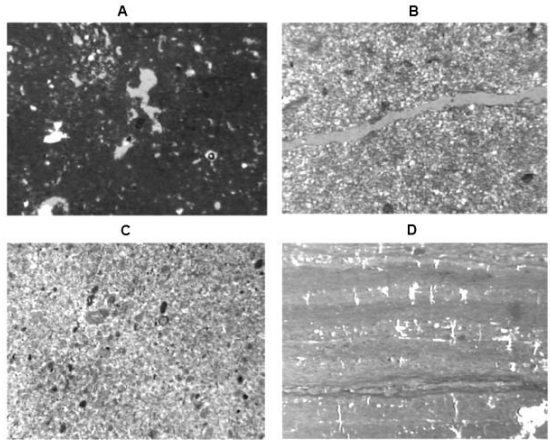


Figure 4. *Photomicrographs of core samples showing various PSTs of the reservoir. (A) Dolomitic mudstone with irregular fenestral fabric, vuggy porosity and anhydrite plugging. Core depth (m): 3004.86, magnification: 120×, PPL, helium porosity (%): 21.79, air permeability (mD): 3.9. (B) Fine to very fine-grained peloidal dolograinstone with fracture, interparticle and intercrystalline porosity types. Core depth (m): 2953.72, magnification: 47×, PPL, helium porosity (%): 16.89, air permeability (mD): 21.82. (C) Fine to very fine peloid dolograinstone with few skeletal debris and a few inter-particle porosity. Core depth (m): 3247.10, magnification: 23×, PPL, helium porosity (%): 3.32, air permeability (mD): 0.1. (D) Laminated stromatolite boundstone with laminoid fenestral fabric and micro-mud cracks. Core depth (m): 2946.85, magnification: 23×, PPL, helium porosity (%): 1.53, air permeability (mD): 0.17 (Modified from Karimpouli et al., 2013).*

Figure 5 is the cross plot of porosity versus frame flexibility factor representing lithology types. It is evident that each lithology contains different types of pore structure. In this study, we found that there are both positive and negative values for γ. According to the formula of γ, this occurs when the sample has very low porosity. Core analysis results showed that the dominant lithology of the samples with negative value of γ is usually anhydrite, compact limestone or dolomite which are considered low porosity rocks (Figure 5). Vuggy and fracture porosities have low positive γ values with a softer structure (Sun, 2004) suitable for gas storage (Figure 6(A)). These two porosity

types (i.e. vuggy and fracture) mostly contain gas as the dominant fluid (Figure 6(B)). We consider them as PST1.With increasing γ value, it is seen that cracks and micro-fracture porosity types are the dominant pore structures having medium to low porosity. We consider them as the second pore space type (PST2) containing a mixture of gas and brine. As previously mentioned, low porosities cause negative values for γ. The third porosity space type, PST3, is the micro-porosity containing only brine (Figure 6(A)).

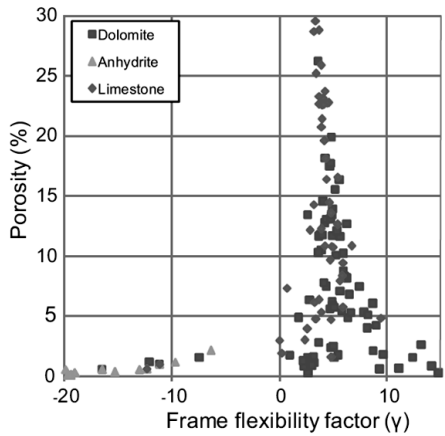


Figure 5. *Cross-plot of porosity-frame flexibility factor for different lithologies (Modified from Karimpouli et al., 2013).*

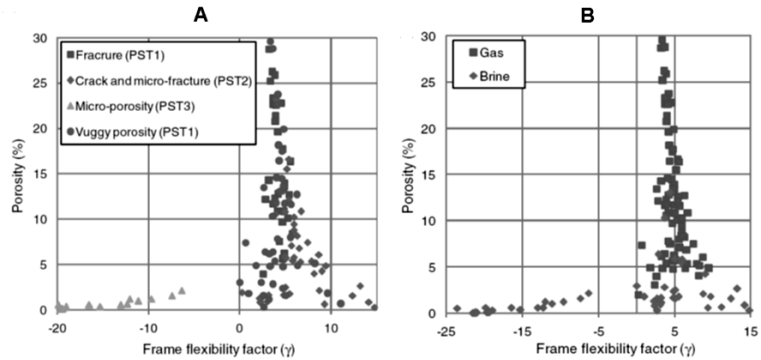


Figure 6. *Cross-plot of porosity-frame flexibility factor for (A) different PSTs and (B) fluid content (Modified from Karimpouli et al., 2013).*

According to Sun (2004), although porosity and γ can be mathematically independent, the distributions of pore types in naturally occurring rocks are likely to be statistically related to the porosity distribution, depending on the formation history and diagenesis. Thus, the cutoffs of the γ value for different PST classifications may vary in different reservoirs; therefore, core data are required to calibrate the inverted frame flexibility factor to determine its cutoffs for pore type classification on the velocity-porosity cross plots (see Dou et al., 2011). On the basis of the calibration of the cutoffs for γ in this reservoir, we concluded that the γ values between 0 and 5 are the best class for vuggy and fracture porosities. Consequently, microporosities are classified by $\gamma > 0$, and cracks and microfractures are classified by $\gamma < 5$ Using this classification, scattering of velocity-porosity trends decreased in different classes, and better linear relations were able to be fitted.

The cross-plot of P-wave velocity versus porosity classified by γ is shown in Figure 7. As was expected, data show a negative trend implying that P-wave velocity decreases when porosity increases. Moreover, P-wave velocity shows a wide-scattered range. For example, it varies about 700 m/s at about 13% porosity. However, using a classified range of γ, porosity-velocity trends are classified based on geological evidence such as pore space types (PSTs) and rock texture, which produce a more accurate trend and prediction of porosity.

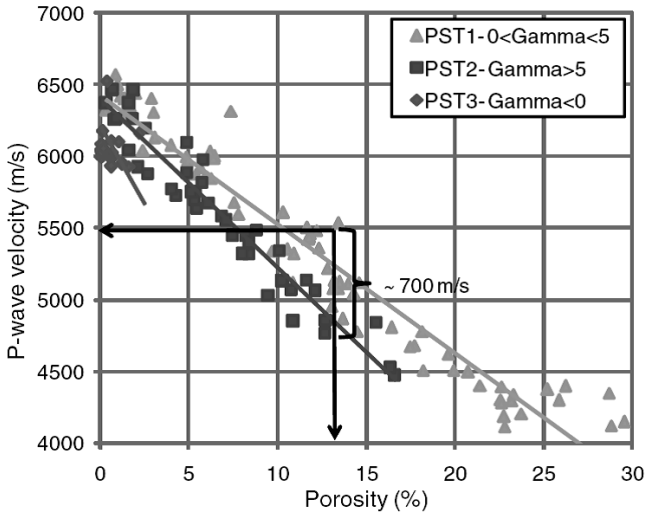


Figure 7. *Cross-plot of P-wave velocity-porosity. Velocity varies about 700 m/s at a porosity about 13%. Classification of the data based on PSTs shows a clear relationship between the velocity and porosity (Modified from Karimpouli et al., 2013).*

3.5 Implementation of Bayesian Facies Estimation

After selecting and calculating the proper parameters of the carbonate reservoir (i.e. ϕ, γ, K_f), they were predicted from pre-stack data in a complete Bayesian framework and then could be used to predict different facies according to the following steps.

Elastic parameters were inverted on a seismic scale using Bayesian linearized AVO inversion by Buland and Omre (2003) on well-A. Pre-stack seismic data were available at four angles, namely 6◦, 16◦, 26◦ and 35◦ in a depth interval between 2818 and 3258 m (i.e. the reservoir zone). Data for the 35◦ angle show a very low quality and, therefore, were not used in this study. Prior to the inversion, time-to-depth conversion and wavelet extraction were carried out to tie the

reflections with the following well data steps (Malehmir et al., 2012):

- Seismic data were first time-to-depth converted using available checkshot-corrected well velocity information.
- Acoustic impedance logs were calculated and used to derive well reflectivity.
- A constant phase wavelet (frequency-independent) was estimated statistically from the input seismic data and used to generate synthetic seismograms.
- To better correlate the synthetic with the observed seismic data, the stretch and squeeze method was applied on the synthetic seismograms.
- An updated wavelet was then extracted for tying the reflections to the well data using an iterative manner. Finally, a wavelet for each angle was extracted (Figure 8).

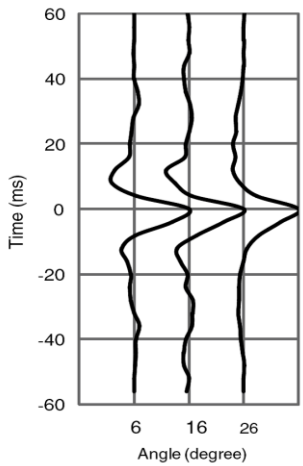


Figure 8. *Extracted wavelets at different angles from pre-stack data.* (Modified from Karimpouli et al., 2013).

Synthetic data were generated for noise estimation by Aki-Richard's

approximation of the Zoeppritz equation and convolved with extracted wavelets for each angle. A comparison between the real seismic (Figure 9A) and the synthetic data (Figure 9B) suggests that the pre-stack data are highly noisy and their quality is very low. This has a detrimental effect on the interpretation of data in the reservoir as almost no inversion method produces acceptable results, especially for the inversion of S-wave velocity and its derivatives (personal communication to NIOC 2012). However, Figures 9(C) and 9(D) show that the Bayesian method produces reasonable results for the inversion of P- and S-wave impedances in well-A. To evaluate the efficiency of Bayesian inversion, this method was compared with the model based inversion method (Russell and Hampson, 1991) which is illustrated in Figures 9(E) and 9(F). According to these results, Bayesian method did a better job. However, RMS error, calculated for both methods, showed that Bayesian method inverted the P- and S-wave impedances, 5% and 12% better than the model based method, respectively. A validation of this method was made using well-B data as illustrated in Figure 10, which confirms that this method is valid enough to be used for inversion of elastic parameters.

In the next step, petrophysical parameters ($R = \left[\phi, \gamma, K_f\right]^T$) were inverted on well-A. In terms of the resolution, we expect that layers thicker than 25 m are vertically well resolved (using 50 Hz effective frequency and 5000 m/s velocity). A discrete format of a different probability was produced on the basis of statistical rock physics and was applied according to equation (2). However, the results were not enough promising. We attribute this to the non-uniqueness problem. To overcome this problem, an error term (Er) is defined as the difference between the velocity ratio of a priori data (well-log data) and the computed one:

$$Er = \left| \left(\frac{V_P}{V_S} \right)_{cmp} - \left(\frac{V_P}{V_S} \right)_{pre} \right| \tag{31}$$

The results of the petrophysical parameter inversion in well-A before and after solving the non-uniqueness problem are shown in Figure 11. Porosity is underestimated in comparison to the well data and even in comparison to predicted data before solving non-uniqueness, but it is still relatively reasonable. The two other parameters (i.e. fluid bulk modulus and frame flexibility factor) have obviously been predicted much better using the error term. On the other hand, there is a good match between the well data and the predicted ones especially at the depth interval between 2884 and 3200 m. However, at depths greater than 3200 m, the results are not reliable. This occurs because, with increasing depth, the signal to noise ratio (S/N) of seismic data decreases; therefore, elastic parameters are not accurately inverted (see Figure 9), and then rock physics parameters are poorly estimated.

To validate the efficiency of our method, we used this methodology on the data from well-B. Predicted parameters are shown in Figure 12, confirming the reliability of our method. However, at depths greater than 3150 m, the results bear little meaning. We also attribute this to low S/N and the unreliable inversion of seismic properties (Figure 10).

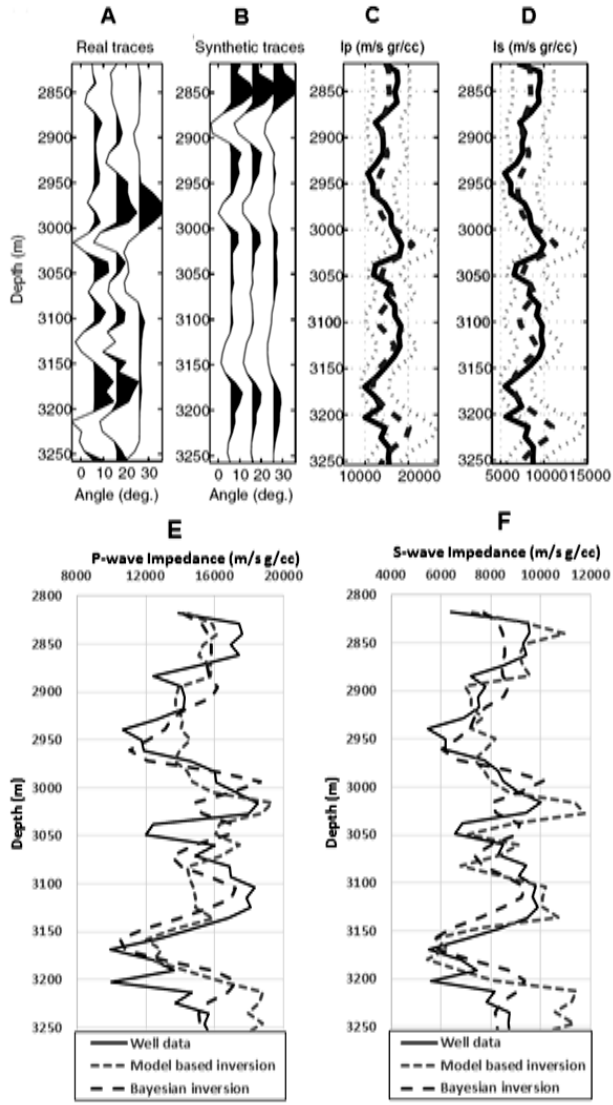


Figure 9. *Bayesian inversion of depth-converted P- and S-wave impedances in well-A. (A) and (B) The real and synthetic seismic data. (C) and (D) P- and S-wave impedances (solid line: well data, long-dashed line: MAP value and small-dashed line: 95% prediction interval). (E) and (F) Inverted P- and S-wave impedances using the Bayesian (long-dashed line) and model based (small-dashed line) inversion methods. RMS error showed that Bayesian method inverted the P- and S-wave impedances, 5% and 12% better than the model based method, respectively. (Modified from Karimpouli et al., 2013).*

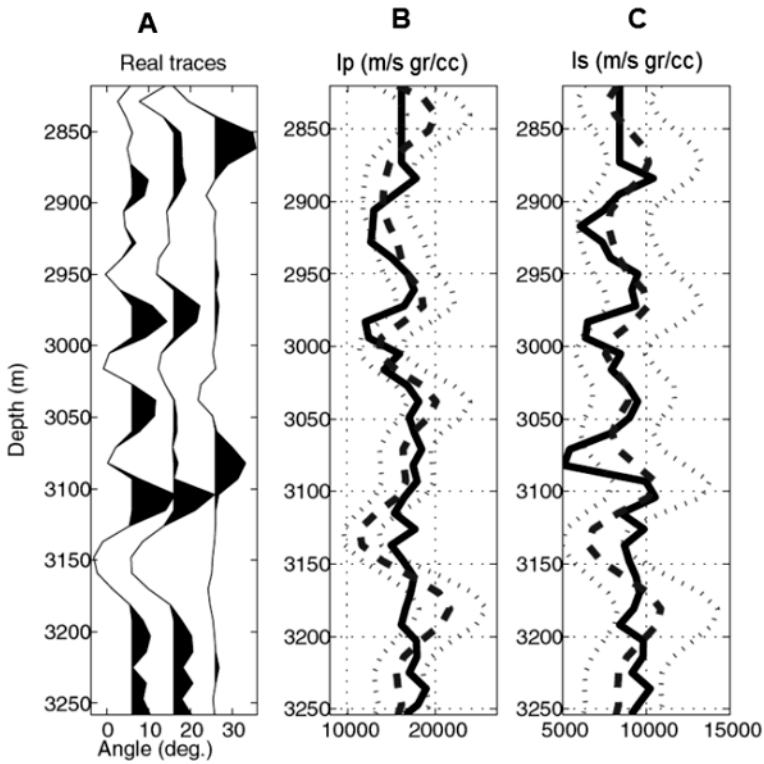


Figure 10. *Bayesian inversion of depth-converted P- and S-wave impedances in well-B. (A) The real seismic data. (B) and (C) P- and S-wave impedances. (Black solid line: well data, red long-dashed line: MAP value and red small-dashed line: 95% prediction interval) (Modified from Karimpouli et al., 2013).*

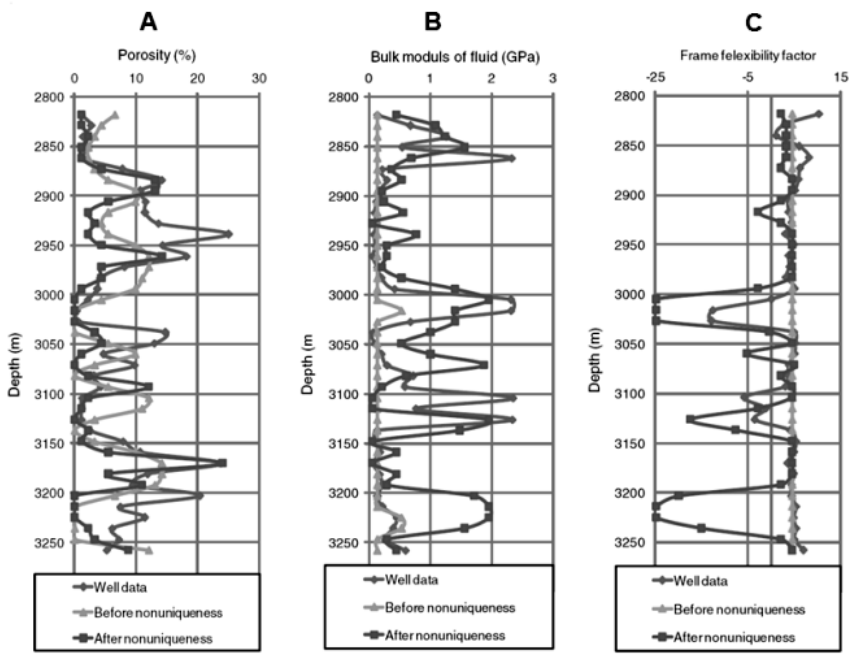


Figure 11. *Plots of real and predicted rock physics parameters: (A) porosity, (B) fluid bulk modulus and (C) frame flexibility factor for well-A. Comparison of predictions before and after solving the non-uniqueness problem with real well data shows the effectiveness of the proposed method (Modified from Karimpouli et al., 2013).*

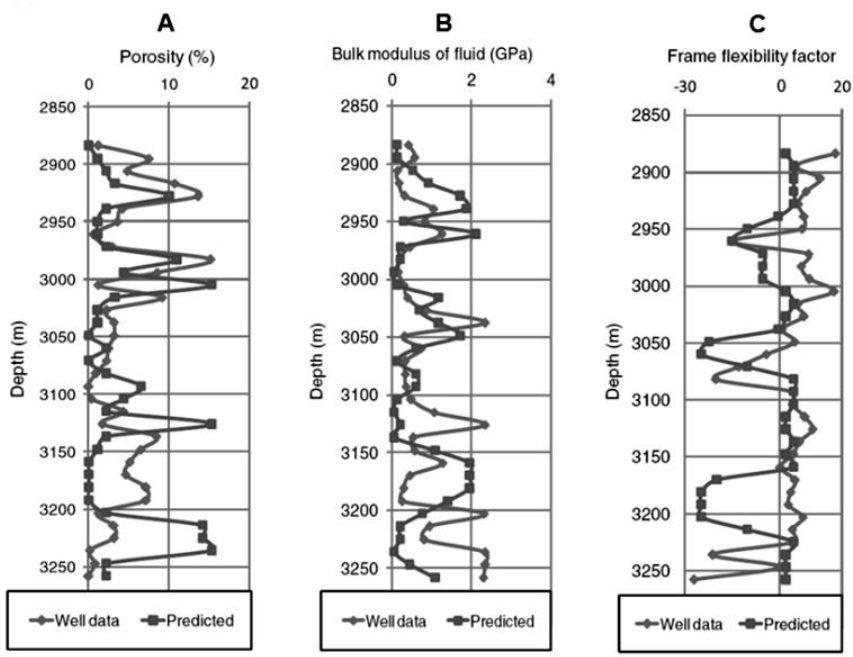


Figure 12. *Plots of real and predicted rock physics parameters: (A) porosity, (B) fluid bulk modulus and (C) frame flexibility factor of well-B (Modified from Karimpouli et al., 2013).*

In the last part, a combination of three mentioned rock physics parameters was used to define different facies (Figure 13). Therefore, a high quality facies is a high porous facies with proper PST-containing gas as the fluid content. Conversely, a low quality facies is a low porous one with improper PST containing brine. Finally, the third facies is the transition between these two end members.

The probability of occurrence of each facies conditioned to the seismic data at each depth (z) can be calculated using eq. (24). It should be mentioned that the Markov chain Monte Carlo (MCMC) sampling method can be a good solution of eq. (24) only in 1D data. In this study, we used the maximum a posteriori (MAP) of eq. (9):

$$(f_z)_{MAP} = \arg\max_{f_z} P(f_z \mid S_z) \tag{31}$$

Figure 14 shows the results of this method. The high quality facies is predicted fairly accurately. Statistically speaking, by using the MAP solution, this facies is accurately predicted in more than 67% of cases and is inaccurately predicted in about 33% of cases. Since the seismic data are highly noisy and of low quality at this depth (see Figure 9), these results are encouraging and still reliable. Low quality facies are in most cases associated with the thin layers in the seismic scale (Figure 14); therefore, it is not predicted in MAP solution. The probability plot shown in Figure 14 suggests that, because the probability of this facies is not high enough, it does not appear in the MAP results.

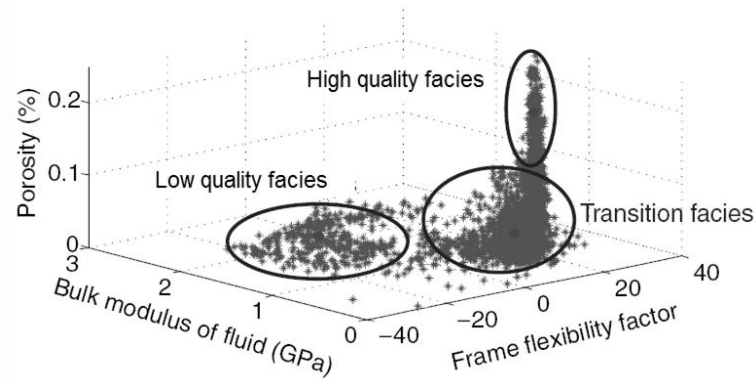


Figure 13. *Distribution of reservoir parameters in well-A, and the classifications of high quality, low quality and transition facies. Non-Gaussian distribution behavior of the data can be captured by Gaussian mixture model with three components. Red dots are the center of these components (Modified from Karimpouli et al., 2013).*

In this study, a 3D cube of prestack seismic data was available in three angles of the incidents: 6, 16 and 26 degrees. This cube is used to predict favourable facies in the reservoir zone. Since the algorithm is trace based, it was easy to generate a 3D cube of favourable facies distribution across the reservoir. Figure 15 shows the final results of high quality facies prediction. According to Figure

15, high quality facies are aggregated into two main layers known as K2 and K4 submembers based on well and seismic data. These results have a good correlation with other studies confirming that these submembers are the main reservoir intervals (Aali et al., 2006; Ehrenberg, 2006; Moradpour et al., 2008; Rahimpour-Bonab, 2007; Rahimpour-Bonab et al., 2009). To have a better illustration of the 3D model, two more sections one in the middle of the model (Figure 16a) and the other in depth (Figure 16b) are shown in Figure 16. Since these data are from reservoir zone, high quality facies have a high frequency.

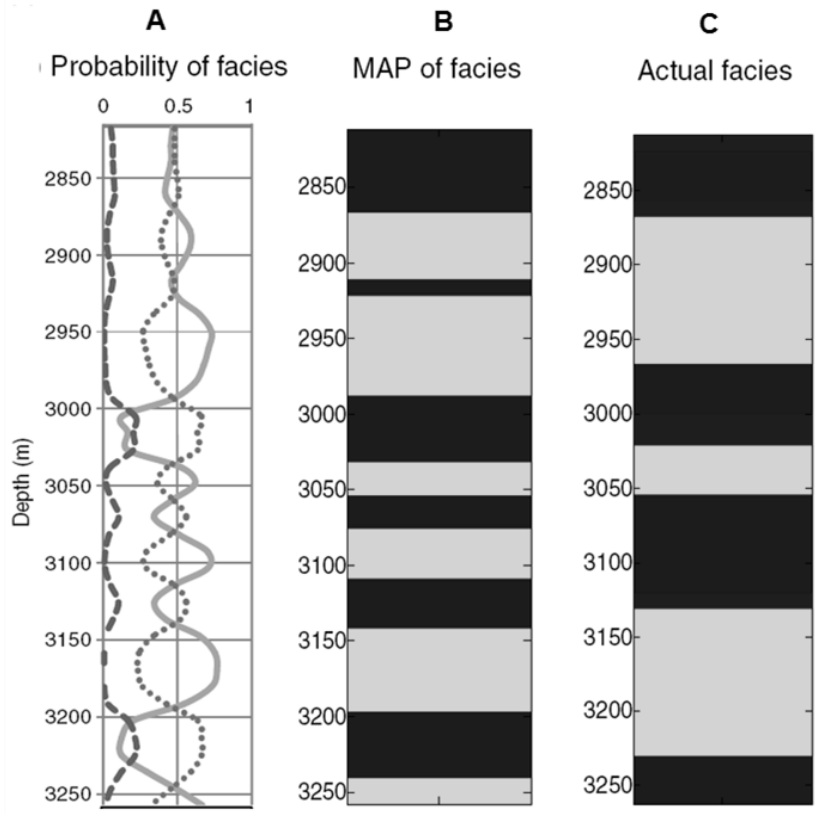


Figure 14. *Final results for probabilistic facies prediction in well-A (light green: high quality, red: low quality, blue: transition facies). (A) Probability plot of conditional occurrence of different facies. (B) MAP of facies and (C) actual facies (Modified from Karimpouli et al., 2013).*

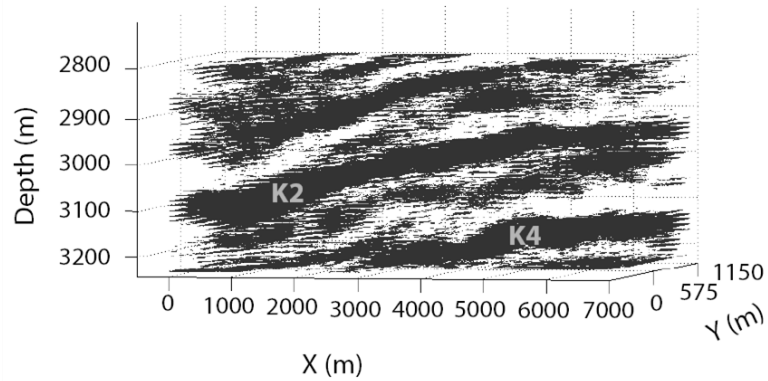


Figure 15. *Maximum a posteriori prediction of high quality facies in a 3D volume. K2 and K4 are the main reservoir submembers confirmed by these results.*

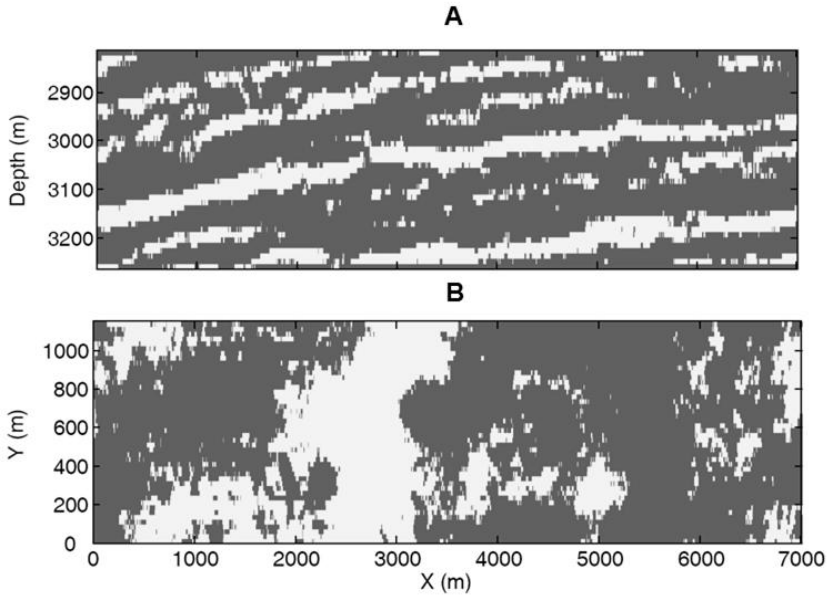


Figure 16. *Maximum a posteriori prediction of high quality facies in (a) Y=550 m and (b) depth of 3000 m.*

3.6 Conclusions

In this study, a carbonate gas reservoir in Iran was studied for probabilistic

prediction of high quality parts of the reservoir at an exploration stage. Porosity, frame flexibility factor and bulk modulus of fluid were chosen as the proper parameters to capture elastic behavior, geological evidence and fluid detection and to classify different facies in carbonate reservoir studies. Based on core studies from the well data, dominant pore types are vuggy, fractures, cracks, micro-fractures and micro-porosities. We concluded that the γ values between 0 and 5 are the best class for vuggy and fracture porosities. Micro-porosities are classified by $\gamma < 0$, and cracks and micro-fractures are classified by $\gamma > 5$. According to the rock physics parameters, three facies were defined. The first, a high quality facies, is a highly porous facies with proper pore structure type and gas as fluid content. In contrast, the low quality facies is a low porosity one with improper pore structure type and brine as fluid content. Consequently, a transition facies is considered between these two end members. To invert desired facies from the seismic data and evaluate their uncertainty, a Bayesian based method was used. Inversion results show good correlation between inverted and true parameters. However, at greater depths, results are not convincing and are attributed to lower signal to noise ratio at depth. Finally, different facies were predicted with their probability of occurrence. The most probable distribution of favourable facies in 3D seismic data has a meaningful relationship with the geological evidence of the reservoir. High quality facies are aggregated into two main layers known as K2 and K4 submembers which, according to the previous studies, are considered as the main reservoir intervals. These results show that Bayesian methods are reliable enough to predict the desired facies with an evaluation of their uncertainties. However, the definition of the facies based on distribution of rock physics parameters can help us to distinguish and classify the high quality facies.

Acknowledgment

We acknowledge NIOC for providing the data and permission to publish them. We also thank Arild Buland and Dario Grana for their helpful comments.

References

[1] Aali, J., Rahimpour-Bonab, H., and Kamali, M.R., 2006. Geochemistry and origin of the world's largest gas field from Persian Gulf, Iran. *Journal of Petroleum Science and Engineering*, 50, 161-175.

[2] Adam, L., Batzle, M., and Brevik, I., 2006. Gassman's fluid substitution and shear modulus variability in carbonates at laboratory seismic and ultrasonic frequencies. *Geophysics*, 71, F173-F183.

[3] Aki, K., and Richards, P. G., 1980. Quantitative seismology. *W H Freeman & Co*.

[4] Anselmetti, F. S., and Eberli, G. P., 1999. The velocity-deviation log: a tool to predict pore type and permeability trends in carbonate drill holes from sonic and porosity or density logs. *American Association of Petroleum Geologists Bulletin*, 83, 450-466.

[5] Assefa, S., McCann, C., and Sothcott, J., 2003. Velocities of compressional and shear waves in limestone. *Geophysical Prospecting*, 51, 1-13.

[6] Avseth, P., Mukerji, T., Jørstad, A., Mavko, G., and Veggeland, T., 2001. Seismic reservoir mapping from 3-D AVO in a North Sea turbidite system. *Geophysics*, 66, 1157-1176.

[7] Backus, G., 1962. Long-wave elastic anisotropy reduced by horizontal layering. *Journal of Geophysical Research*, 67, 4427-4440.

[8] Baechle G T, Eberli G P, Wegar R J and Massaferro L 2009 Changes in dynamic shear moduli of carbonate rocks with fluid substitution *Geophysics* 74 E135-47.

[9] Bosch, M., Mukerji, T., and Gonzales, E. F., 2010. A review to Seismic inversion for reservoir properties. *Geophysics*, 75, A165-A176.

[10] Buland, A., 2002. Bayesian seismic AVO inversion. *PhD thesis*, Norwegian University of Science and Technology. p 159.

[11] Buland, A., and Omre, H., 2003. Bayesian linearized AVO inversion. *Geophysics*, 68, 185-198.

[12] Buland, A., O. Kolbjørnsen, R. Hauge, O. Skjæveland, and K. Duffaut., 2008. Bayesian lithology and fluid prediction from seismic pre-stack data. *Geophysics*, 73, C13-C21.

[13] Dou, Q. F., Sun, Y. F., and Sullivan, C., 2009a. Seismic detection of paleokarst system and its influence on carbonate reservoir compartmentalization. *SEG Expanded Abstract*, 28, 1731-1736.

[14] Dou, Q. F., Sun, Y. F., and Sullivan, C., 2009b. Rock-physics-based heterogeneity characterization of a carbonate reservoir in the Permian Basin. *SEG Expanded Abstract*, 28, 1945-1950.

[15] Dou, Q., Sun, Y. F., and Sullivan, C., 2011. Rock-physics-based carbonate pore type characterization and reservoir permeability heterogeneity evaluation, upper San Andres reservoir, Permian basin, West Texas. *Journal of Applied Geophysics*, 74, 8-18.

[16] Duijndam, A. J. W., 1988. Bayesian estimation in seismic inversion—part I: Principles: *Geophys. Prosp.*, 36, 878-898.

[17] Eberli, G. P., Baechle, G. T., Anselmetti, F. S., and Incze, M., 2003. Factors controlling elastic properties in carbonate sediments and rocks. *The Leading Edge*. 22, 654-660.

[18] Ehrenberg, S.N., 2006. Porosity destruction in carbonate platforms. *Journal of Petroleum Geology*, 29, 41-52.

[19] Eidsvik, J., P. Avseth, H. Omre, T. Mukerji, and G. Mavko, 2004. Stochastic reservoir characterization using pre-stack seismic data. *Geophysics*, 69, 978-993.

[20] Grana, D., and Della Rossa, E., 2010. Probabilistic petrophysicsal-properties estimation integrating statistical rock physics with seismic inversion. *Geophysics*, 75, O21-37.

[21] Grana, D., and J. Dvorkin, 2011. The link between seismic inversion, rock physics, and geostatistical simulation in seismic reservoir characterization study. *The Leading Edge*, 30, 54-61.

[22] Houck, R. T., 2002. Quantifying the uncertainty in an AVO interpretation. *Geophysics*, 67, 117-225.

[23] Karimpouli, S., Hassani, H., Nabi-Bidhendi, M., Khoshdel, H., and Malehmir, A., 2013. Application of probabilistic facies prediction and estimation of rock physics parameters in a carbonate reservoir from Iran. *Journal of Geophysics and Engineering*, 10, 015008.

[24] Larsen, A. L., M. Ulvmoen, H. Omre, and A. Buland, 2006. Bayesian lithology/fluid prediction and simulation on the basis of a Markov-chain prior model. *Geophysics*, 71, R69-R78.

[25] Malehmir, A., Juhlin, C., Wijns, C., Urosevic, M., Valasti, P., and Koivisto, E., 2012. 3D reflection seismic investigation for open-pit mine planning and exploration in the Kevitsa Ni-Cu-PGE deposit, Northern Finland. *Geophysics*, 77, WC95-WC108.

[26] Mavko, G., T. Mukerji, and J. Dvorkin, 2009. The rock physics handbook. *Cambridge University Press*.

[27] Moradpour, M., Zamani, Z., and Moallemi, S. A., 2008.

[28] Controls on reservoir quality in the Lower Triassic Kangan Formation, Southern Persian Gulf, *Journal of Petroleum Geology*, 31, 367-386.

[29] Mukerji, T., A. Jørstad, P. Avseth, G. Mavko, and J. R. Granli, 2001. Mapping lithofacies and pore-fluid probabilities in a North Sea reservoir: Seismic inversions and statistical rock physics. *Geophysics.* 66, 988-1001.

[30] Rahimpour-Bonab, H., 2007. A procedure for appraisal of a hydrocarbon reservoir continuity and quantification of its heterogeneity. *Journal of Petroleum Science and Engineering*, 58, 1-12.

[31] Rahimpour-Bonab, H., Asadi-Eskandar, A., and Sonei, A., 2009. Controls of Permian-Triassic Boundary over Reservoir Characteristics of South Pars Gas Field, Persian Gulf. *Geol. J.*, 44, 341-364.

[32] Roncarolo, F., and Grana, D., 2010. Improved reservoir characterization integrating seismic inversion, rock physics model and petroelastic log facies classification. A real case application. *SPE annual technical conference and exhibition*, SPE 134919.

[33] Russell, B., and D. Hampson, 1991. A comparison of post-stack seismic inversion methods. *Annual International Meeting, SEG, Expanded Abstracts*, 876-878.

[34] Saberi, M. R., 2010. An integrated approach for seismic characterization of carbonates *PhD thesis*, University of Bergen.

[35] Sun, Y. F., 2000. Core-log-seismic integration in hemipelagic marine sediments on the eastern flank of the Juan De Fuca Ridge. *ODP Scientific Results*, 168, 21-35.

[36] Sun, Y. F., 2004. Effects of pore structure on elastic wave propagation in rocks, AVO modeling. *Journal of Geophysics and Engineering*, 1, 268-276.

[37] Sun, Y. F., and Goldberg, D., 1997a. Effects of aspect ratio changes on wave velocities in fractured rocks. *SEG Expanded Abstract*, 67, 925-928.

[38] Sun, Y. F., and Goldberg, D., 1997b. Estimation of aspect ratio changes with pressure from seismic velocities. In: Lovell M A, Harvey P K (Eds.) Developments in Petrophysics *Geological Society Special Publication*, 122, 131-139.Tarantola A 2005 *Inverse Problem Theory and Methods for Model Parameter Estimation* (Philadelphia, PA: SIAM).

[39] Tarantola, A., 2005. Inverse problem theory and methods for model parameter estimation. *Society for Industrial and Applied Mathematics*.

[40] Tavakoli, V., Rahimpour-Bonab, H., and Esrafili-Dizaji, B., 2011. Diagenetic controlled reservoir quality of South Pars gas field, an integrated approach. *C. R. Geoscience*, 343, 55-71.

[41] Tiwary, D. K., I. O. Bayuk, A. A. Vikhorev, M. Ammerman, and E. M. Chesnokov, 2007. Comparison of seismic upscaling methods. *SEG Expanded Abstracts*, 77, 1933-1936.

[42] Ulrych, T. J., Sacchi, M. D., and Woodbury, A., 2001. A Bayes tour of inversion: A tutorial. *Geophysics*, 66, 55-69.

[43] Ulvmoen, M., and Omre, H., 2010. Improved resolution in Bayesian lithology/fluid inversion from pre-stack seismic data and well observations: Part 1-Methodology. *Geophysics*, 75, R21-R35.